# DAMAGE EVOLUTION ASSESSMENT OF COMPOSITES WITH EMBEDDED FIBRE OPTICS BY MEANS OF MICRO COMPUTED TOMOGRAPHY

G. Chiesura*[1], G. Luyckx[1], E. Voet[1], N. Lammens[1], W. Van Paepegem[1], J. Degrieck[1], M. Dierick[2], L. Van Hoorebeke[2], P. Vanderniepen[2]

[1] *Department of Material Science and Engineering, Ghent University, Technologiepark 903, 9052 Zwijnaarde, Belgium*
[2] *UGCT – Department of Physics and Astronomy, Ghent University, Proeftuinstraat 86, 9000 Ghent, Belgium*
** e-mail address of the corresponding author: gachiesu.Chiesura@ugent.be*

**Keywords:** Optical Fibre Sensor, Carbon fibre, Defects, Radiography, Autoclave, Prepreg.

**Abstract**
*In this work different optical fibre sensors (e.g. different diameter and coating thicknesses) have been embedded in a prepreg carbon fibre/epoxy laminate and manufactured by autoclave process. Strains built up after curing (i.e. cooling down) induced cracking through the coating for some sensors. Some samples were cut out from the laminate and subsequently fatigue loaded to failure. The damage evolution has been followed up at regular intervals by means of a non-destructive technique, known as Micro Computed Tomography. No significant evidence of cracks evolving around the sensors has been found. The damage was bound to its original dimension for the sensors which presented an initial coating crack.*

## 1. Introduction

It is commonly known that the handling (i.e. strain to failure) of optical fibres significantly increases when properly coated [1], [2]. However, when embedded, one should be aware that using the wrong coating material or the incorrect coating thickness could already lead to an undesired damaged state of the hosting material (i.e. composite) in the vicinity of the sensor (i.e. optical fibre) [3], [4]. In literature the coating optimization study has been widely investigated using numerical approaches. Yuan et al. [5] have developed a theoretical model to study the mechanical behaviour of the interface between an embedded optical fibre with an applied coating material and a linear strain matrix. Hadijprocopiou et al. [6] have optimized via a parametric finite element analysis the thermal and mechanical properties of the interface coating that minimize the stress concentration in the host around the sensor. Barton et al. [7] have selected a glass fibre reinforced polymer cross-ply laminate and studied the influence of different coating thicknesses and elastic modulus at different embedding positions through the laminate thickness.
However, a main limitation of such a complete optimization is represented by the technological impracticability in having the correct coating material available (i.e. stiffness), or obtaining the exact coating thickness. Furthermore, also other properties become relevant for a coating selection: the mismatch in thermal expansion coefficients and the maximum process temperature, for instance, are affecting the allowable amount of residual strain that the host can withstand

without initiating a crack. Some commercially available coating materials for fibre optic sensing applications are Acrylate, Polyethylene (PE), Polyamide (PA) or Ormocer (ORganic MOdified CERamics); their moduli of elasticity ranges from 0.8 GPa of the PE family to 3.2 GPa of PA family [8], [10].

This work uses an experimental approach to study the effect of different coating thicknesses on the damage state of a composite in the vicinity of an optical fibre. Ideally, no effects should be noticeable. A set of optical fibres with different diameters and an applied Ormocer coating has been embedded in a carbon fibre laminate. The internal state of the composite around the sensor has been visualized through X-ray micro tomography (µCT). This non-destructive inspection technology uses X-rays to investigate the internal state of a material and has shown to fulfil the requirements of a micro-structural analysis at high resolution (i.e. 2 µm) on composite materials. An initial scan is already taken after manufacturing to investigate the influence of residual stresses on the optical fibre sensor surrounding the composite.

Furthermore different samples have been prepared for testing and have been fatigue loaded to failure. µCT scans have been conducted on the samples at defined intervals to check the damage evolution around the sensor. Summarizing, this work addresses questions related to the sensor/composite interaction for a long term use of a composite structure and, at the same time, it strengthens the use of the micro computed tomography technology for non-destructive inspections on composite materials.

## 2. Materials and methods

### *2.1 Sample Production and Preparation*

A carbon fibre prepreg (i.e. M55J-M18 by Hexcel) cross-ply laminate with a $[90_2,0_2]_{2s}$ lay-up was manufactured by autoclave, using a 2 hours curing temperature of 180 °C and vacuum level of -80 kPa. In order to homogenise the temperature in the laminate, a 20 minutes dwell step at 120 °C was added during the heating up; during the 2nd heating up stage from the dwell to the curing temperature, an external pressure of 7 bars was applied, in order to allow the flowing of the excess resin over the breather material. In the mid layer of the laminate, optical fibre sensors (OFS) with different diameters were embedded aligning them to the reinforcing fibres (i.e. 0° layers). In total 5 rectangular samples, having the following dimensions *t x w x l = 2 mm x 10 mm x 250 mm*, were cut from the laminate and tested under fatigue. In Figure 1 (left) a snap of the fibre optic embedment procedure is proposed.

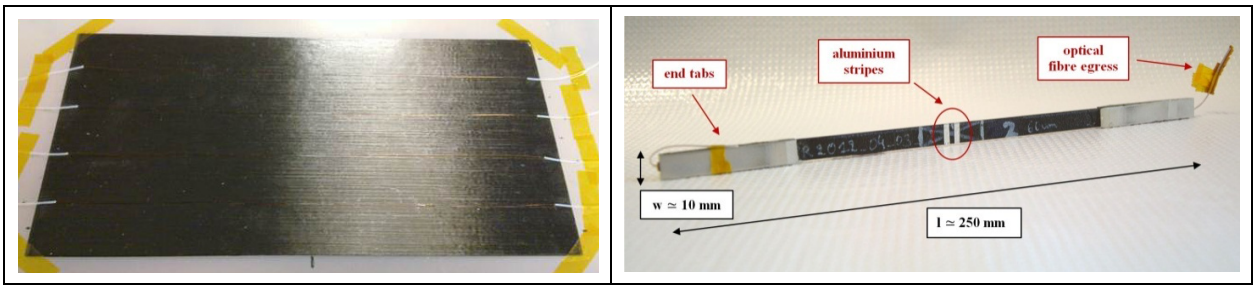


**Figure 1.** Snap of the stacking operation, the fibre optics were protected with some Teflon tubing at the egress points of the laminate (left). Top view of a sample provided with end tabs and ready to be tested (right).

The fibres egress points were protected with some Teflon tubing, this with the only purpose of having a fibre reference position; no strain measurements were recorded from the fibre optic sensors during the fatigue tests. In order to study the damage evolution inside the samples, μCT scans were performed before and after every test sequence. The central zone circled in Figure 1 (right) represents the location where the μCT scans were performed. Some aluminium tape stripes helped as boundary to define the scanning region and were kept glued on the samples during fatigue testing, hence allowing each time scanning the same spot and follow up the damage evolution. As can be noticed from the same figure, the width of the sample was limited to about 10 mm due to restrictions imposed by the μCT setup, as will be discussed in the following.
In Table 1, an overview of the geometric dimensions for the samples tested, with their relative OFSs references, is presented. In samples 1 and 2 a 60 μm diameter optical fibre has been embedded, both samples 5 and 8 have an 80 μm diameter sensor, but sample 8 has a thicker coating. Sample 9 has a 125 μm diameter, while the outer coating diameter is almost equal to the one of sample 8. The b/a ratio is here defined as the ratio between the coating outer diameter and the cladding diameter and represents the parameter to control in order to minimize stresses distribution. In the current work this varies from 2.34 for a fibre with 2 coating layers, to 1.45. For the 60 μm diameter fibre the smallest coating thickness achievable was limited to 106 μm (b/a = 1.76) due to technological reasons. All the optical fibres were coated with Ormocer through a process known as draw tower grating. This procedure simultaneously draws the fibre from the preform to its final diameter, writes the grating and coats it directly after the grating inscription in a continuum manner.

| **Sample n°** | **Sensor Diameter** | **Coating Diameter** | **b/a Ratio** | **Width** | **Thickness** | **Gage Length** |
|---|---|---|---|---|---|---|
| | *[μm]* | *[μm]* | | *[mm]* | *[mm]* | *[mm]* |
| 1 | 60 | 106 | 1.76 | 9.53 | 1.8 | 146 |
| 2 | 60 | 106 | 1.76 | 9.54 | 1.79 | 151 |
| 5 | 80 | 116 | 1.45 | 9.95 | 1.86 | 145 |
| 8 | 80 | 190 | 2.34 | 8.92 | 1.93 | 147 |
| 9 | 125 | 195 | 1.58 | 9.06 | 1.78 | 143 |

**Table 1.** Overview of tested samples and embedded OFS main dimensions.

### *2.2 Fatigue testing method*

In order to define the load limits to apply at the fatigue cycle, a preliminary set of static tensile tests has been performed on 3 reference specimens, which were cut from the manufactured plate according to the ASTM D3039 standard. The average ultimate tensile stress (UTS) was 830±40 MPa. A tension-tension sinusoidal load cycle with a load ratio R of approximately 0.1 was chosen in order to avoid compression on the sample, thus preventing from buckling which may cause premature damage; the load was applied aligned with the fibre optic direction. The cycling frequency was set conservatively to 5 Hz in order to avoid any hot spot region in the polymer matrix. A 100 kN servo hydraulic tensile machine from Instron was used for the tests. The initial

stress level was set between 50 and 450 MPa (~50% of the UTS) for a cumulative of 1,000 cycles. The sample was subsequently dismounted from the test bench and moved to the µCT facility for the scan. The cycle was then resumed at the same stress level till 1,000,000 cycles. Since no evident damage was found after this last stage, the load level was increased to 600 MPa (~70% of the expected UTS) and cycled for another 1,000 cycles, resulting in a cumulative of 1,001,000 cycles. The following load cycles were continued at the same stress level till 2,000,000 cycles and, as last, till 4,000,000 cycles. Before and after any load cycle, a static test was performed to check for a stiffness degradation and therefore control the damage evolution. The axial deformation on the sample during these checks was recorded using an extensometer.
At every cycle stop, as well as for the initial and final conditions, a micro-CT scan was performed on each sample, in order to examine the internal integrity of the material in a delimited volume around the OFS. In the next section, an overview of the µCT facility is provided for completeness.

### *2.3 Micro-CT setup*

The scans were obtained using a modular 900 nm CT scanner, property of the UGCT – Centre for X-ray Tomography of Ghent University [11]; an overview of the facility is given in Figure 2. The sample is fixed on a high precision piezo-positioning manipulator and rotates, allowing to obtain projections at different orientations. The X-ray tube is a FXE-160.50 dual head open type source from Feinfocus, with medium energy (up to 160 keV) and maximum power of 150W. The detector chosen for the proposed applications is a Varian 2520V Paxscan a-Si flat panel with 1820 *x* 1460 pixels, 127 µm pixel size, covering a 20 *x* 25 $cm^2$ area. The sample manipulator is an XYZ-theta CT system with ultra-precision air-bearing rotation motor from MICOS (UPR-160F AIR). The X-ray source was selected at 100 kV and 3 Watt of target power, resulting in a voxel pitch of 2 µm (i.e. resolution of the cross section images). In total 1500 projections were recorded over 360° and the data were reconstructed with the in-house developed Octopus software package. The reconstructed pictures were post-processed through Mathcad and analysed, while 3D renderings were made with VGStudio Max from the original reconstructed images [12].

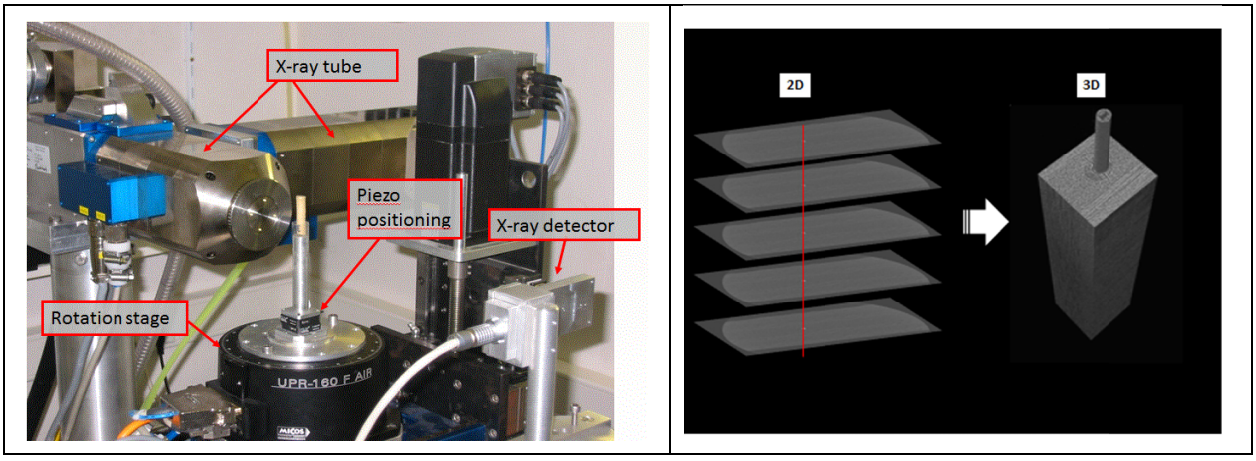


**Figure 2:** (left) Modular 900nm Micro Computed Tomography (micro-CT) scanner of UGCT used in the current work, (right) schematic showing the reconstruction of a 3D scanned volume from a stack of 2D cross sections.

## 3. Experimental results

### *3.1 Initial state after curing*

The scans presented in this section are taken after production and preparation of the samples, meaning that no mechanical load was yet applied. Figure 3 (top-right) is the result of a post processing algorithm applied on a stack of 200 cross sections taken approx. from the middle scanned volume. Each cross section is translated and rotated with respect to the OFS axis and the entire stack is then averaged and filtered in order to reduce noise and increase sharpness. The cross section corresponds approx. to a region of 4 *x* 2 mm$^2$. One can distinguish between the 0° and the 90° oriented layers; every layer is composed of two plies about 200 µm thick each. The mid layer has four 0° plies and the optical fibre is embedded in the centre. The sideways contours are curved due to the limited detector screen area, while the upper and lower edges belong to the sample top and bottom surfaces. One can also note a richer resin film at each 0/90 interface layer: a darker colour is the result of a lower X-ray attenuation, meaning a lower density, which corresponds to a richer resin content region.

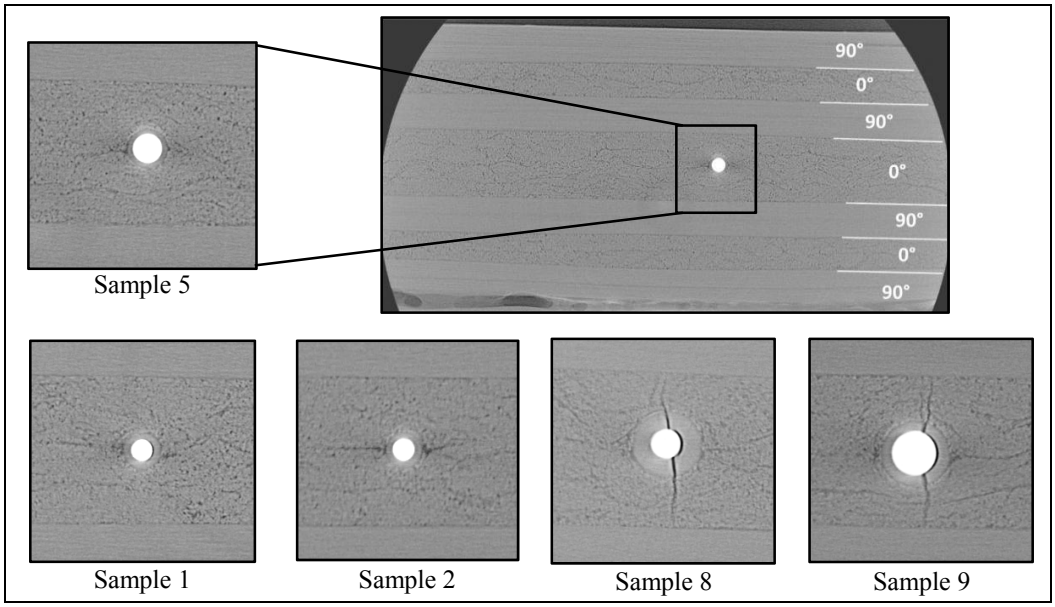


**Figure 3.** (top-right) The result of a post-processed image from an averaging of approx. 200 reconstructed 2D cross sections taken from the middle scanned region for sample 5. The entire area corresponds roughly to 4 *x* 2 mm$^2$; there is a clear distinction between 0° and 90° layers. (top-left) Enlargement of the area surrounding the OFS (500 *x* 500 µm$^2$) for sample 5. (bottom) Enlargement of the area surrounding the OFS for all the other samples.

The enlargement of the sensor surroundings (Figure 3 top-left and bottom) highlights already damages around the optical fibre for some of the samples. A transversal crack is evolving through the coating of the sensor towards the interface with the nearest 90° layers in sample 8 and 9, which have, respectively, an 80 µm fibre with thicker coating and a standard 125 µm fibre embedded. Though not immediately visible, a de-bonding at the OFS-coating interface for the 60 µm OF (sample 1) is present. Sample 5 presents no crack and results in a better coating-composite, as well as a coating-cladding, adhesion. A point of interest ensues from the plies redistribution around the sensor creating richer resin areas sideways and, at the same time,

compacting the reinforcing fibres above and below the sensor, resulting in a higher local fibre volume fraction. The richer resin areas appear more marked for the smaller sensor, but at the same time the distortion of the plies around it appears less important. For the same reason in sample 9 the 0° plies are pushing the closest 90° ones, thus slightly distorting the whole layup.

*3.2 Damage evolution*

Beside the important result of the initial state after curing shown in the previous section, we also investigated the overall damage evolution, through the thickness of the laminate. This was possible by analysing the 3D model rendered from the scanned volume. In order to give a quantitative evaluation of the damage occurring during fatigue testing, it was chosen to count the number of cracks present in a cross section passing through the axis of the optical fibre. An overview of a section extracted from the 3D rendered volume for one of the scanned sample is presented in Figure 4 for clarity.

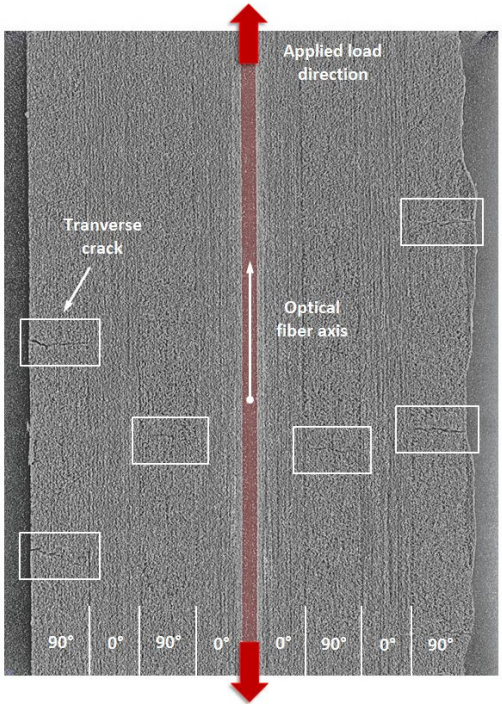


**Figure 4.** Example of a section – taken along the optical fibre axis – extracted from the 3D rendered volume of a micro-CT scan. The sample shows some transverse cracks (i.e. matrix cracking) in the 90° layers, as highlighted in white boxes; the red strip in the centre is the optical fibre.

Due to the cross-ply layup and the loading conditions, the cracks were initiated in the 90° layers transversely to the direction of the applied force [13]. The different sections were analysed and compared at different number of cycles for each sample. Table 2 resumes the number of transverse cracks counted in these sections.

| Sample | 0 cycle | 1000000 cycles | 1001000 cycles | 2000000 cycles | 4000000 cycles |
|---|---|---|---|---|---|
| 1 | 0 | 6 | 8 | 19 | 23 |
| 2 | 1 | 10 | 11 | 21 | 30 |
| 5 | 3 | 12 | 13 | 20 | 24 |
| 8 | 2 | 11 | 17 | 21 | 26 |
| 9 | 5 | 11 | 13 | 22 | 30 |

**Table 2.** Number of cracks counted on a section passing along the axis of the OFS for increasing number of cycles.

An increase in the number of cracks in the 90° layers during evolution of the fatigue cycles is clearly noted. Besides this, no evolution of damage in the central 0° layer (i.e. interlaminar cracks) was noticed.

## 4. Conclusion and outlook

For a given combination of hosting material and fibre optic coating material, an optimum b/a ratio (i.e. ratio between coating and cladding diameters) is foreseen. In this work a carbon fibre epoxy hosting material combined with an Ormocer coated silica fibre was selected. It is evident how an OFS having a large diameter can affect the integrity of the hosting material when embedded, generating a crack, which propagates from the sensor towards the composite. This is certainly true when considering thermal stresses induced in an autoclave cycle during cooling down to room temperature. The same applies to the case of a greater coating thickness, associated with a larger b/a ratio.
Moreover, when considering a smaller diameter OFS (i.e. 80 μm fibre with smaller coating diameter and 60 μm fibre), the induced thermal stress level is not sufficient to induce any damage. However, the result for a 60 μm OFS having a b/a ratio greater than the optimal (i.e. 1.76 in place of 1.45) shows a cladding coating debonding in one of the two samples. This may ensue from the fibre wetting and adhesion during the coating production phase, since the wetting is dependent on the surface geometry and viscosity [14]. However, at this stage of the research, it is not yet clear whether the crack is initiated at the cladding/coating interface, or at the coating/composite interface.
Furthermore, one can address some conclusions on the damage evolution in the middle 0° layer; no evident crack growth around the OFS is detectable after 4 million fatigue cycles. For these situations where there was already a crack present after production, no further evolution of the damage was recognized. Moreover, one cannot associate a larger diameter fibre with a higher number of cracks, since the values shown in Table 2 are scattered. This allows us to conclude that even larger diameter OFS are not affecting the overall life time of a carbon fibre cross-ply laminate which undergoes tensile fatigue loading.

## Acknowledgments

The research leading to these results has received funding from the European Union Seventh Framework Programme FP7/2007-2013 under grant agreement n° 257733 (SmartFiber) and from the Flemish Agency for Innovation by Science and Technology (IWT) – through the program for Strategic Basic Research (SBO) under grant agreement n° 120024 (Self Sensing Composites).

The author gratefully acknowledges also the significant support of UGCT – the "Centre for X-ray Tomography" of Ghent University.

## References

[1] *J. M. Stevens and A. Keough*, The Application OF UV Coatings To Glass Optical Fibre, *The Association for Finishing Processes of SME*, FC78-551, 1978.

[2] *T. Wei*, The Effects of Polymer Coatings on the Strength and Fatigue Properties of Optical Fibres, *Proceedings of American Ceramics Society*, Chicago, Illinois, 1986.

[3] *G. Luyckx, E. Voet, N. Lammens, J. Degrieck*, Strain Measurements of Composite Laminates with Embedded Fibre Bragg Gratings: Criticism and Opportunities for Research, *Sensors*, 11: 384-408, 2011.

[4] *K. Shivakumar and L. Emmanwori.* Mechanics of failure of composite laminates with an embedded fiber optic sensor, *Journal of Composite Materials,* 38(8):669–680, 2004.

[5] *L. B. Yuan, L. M. Zhou, and J. S. Wu*, Investigation of a coated optical fibre strain sensor embedded in a linear strain matrix material, *Optics and Lasers in Engineering*, 35(4):251–260, 2001.

[6] *M. Hadjiprocopiouy, G. T. Reedyx, L. Hollawayz and A M Thorne,* Optimization of fibre coating properties for fibre optic smart structures*, Smart Materials and Structures*, (5):441–448, 1996.

[7] *E. N. Barton, S. L. Ogin, A. M. Torne, G. T. Reed,* Optimisation of the coating of a fibre optical sensor embedded in a cross-ply GFRP laminate, *Composite: Part A*, 33:27-34, 2002.

[8] *M. Honjo and S. Masuda*, Required Properties of UV Curable Resin for Optical Fibre, *Proceedings of Radiation Curing Asia*, Tokyo, Japan, pp. 169-172.

[9] *H. N. Vazarani, H. Schonhorn and T. T. Wang*, Coatings and Plastics Preprints*, Journal of American Chemical Society*, 37(2): 253, 1977.

[10] H. Kuzushita, T. Zushi, T. Watanabe, K. Imamura and H. Tanaka, *Study On Transmission Characteristics Of UV Curable Resin-Coated Optical Fibres At Low Temperatures*, Proceedings of the 36th International Wire & Cable Symposium, Washington D.C., Maryland, 1987.

[11] *B.C. Masschaele, V. Cnudde, M. Dierick, P. Jacobs, L. Van Hoorebeke, J. Vlassenbroeck,* UGCT: New x-ray radiography and tomography facility, *Nuclear Instruments & Methods in Physics Research Section a-Accelerators Spectrometers Detectors and Associated Equipment*, 580(1):266-269, 2007.

[12] *J. Vlassenbroeck, M. Dierick, B. Masschaele, V. Cnudde, L. Hoorebeke, and P. Jacobs,* Software tools for quantification of X-ray microtomography*, Nuclear Instruments & Methods in Physics Research Section a-Accelerators Spectrometers Detectors and Associated Equipment*, 580(1): 442-445, 2007.

[13] *J. M. Berthelot, A. El Mahi, J.F. Le Corre,* Development of transverse cracking in cross-ply laminates during fatigue tests*, Composites Science and Technology,* 61(12):1711–1721, 2001.

[14] *T. T. Wang and H. M. Zupko,* Long-term Mechanical Behaviour of Optical Fibres Coated with a UV-Curable Epoxy Acrylate*, Journal of Materials Science,* 13:2241-2248, 1978.